

# PERFORMANCE EVALUATION OF NON-LINEAR MIMO PRECODERS UNDER TRANSMIT IMPAIRMENTS

José P. González-Coma, Paula M. Castro, José A. García-Naya, and Luis Castedo

Universidade da Coruña, Campus de Elviña s/n, 15071. A Coruña, Spain  
Email: jgonzalezcoma@gmail.com, {pcastro, jagarcia, luis}@udc.es

## ABSTRACT

This work analyzes the impact of radio frequency transmitter impairments on the performance of *Multiple-Input Multiple-Output* (MIMO) systems with nonlinear Tomlinson-Harashima and vector precoding. This analysis is carried out by means of simulation results using two sorts of scenarios: spatially-white Rayleigh channels and measured indoor channels. We also show that incorporating the transmitter noise in the precoder design produces a significant performance improvement.

## 1. INTRODUCTION

Practical implementations of wireless communication transmitters suffer from a large number of impairments such as quantization noise, sampling offset, phase noise, I/Q imbalance ..., which are normally ignored when designing *Multiple-Input Multiple-Output* (MIMO) signaling methods. However, it is shown in [1, 2] that noise generated at the transmitter can significantly affect predicted MIMO system performance. In this work, the impact of residual transmitter noise is evaluated by means of two sorts of scenarios: spatially-white Rayleigh channels and measured indoor channels obtained using a MIMO testbed developed at the University of A Coruña [3]. This latter scenario is specially outstanding to illustrate the influence of transmitter noise on real-world situations. We only consider MIMO nonlinear schemes since their performance is clearly much better than the respective linear ones. More specifically, we focus on *Tomlinson-Harashima Precoding* (THP) [4, 5] and *Vector Precoding* (VP) [6]. THP solves the malicious effect of feeding back wrong decisions inherent to the wellknown *Decision Feedback* (DF) receivers by performing a similar task at transmission. Correspondingly, VP performs a lattice search at transmission similar to that carried out by *Maximum Likelihood* (ML) detectors. Contrary to linear precoders, transmitter impairments significantly affect the performance of nonlinear THP and VP [7, 8]. However, we will show that this performance degradation can be greatly alleviated if the transmitter noise is incorporated in the precoder design.

This work is organized as follows. Section 2 describes the way of modeling the aforementioned transmitter impairments. Sections 3 and 4 respectively explain the design of THP and VP when transmitter noise is included into filter optimizations. Finally, computer simulations are shown in Section 5 and some concluding remarks are stated in Section 6.

## 2. SIGNAL MODEL WITH TX-NOISE

When considering a non-ideal transmitter affected by residual transmitter noise, the transmitted symbols are modeled

as

$$\mathbf{x}_t[n] = \mathbf{x}[n] + \boldsymbol{\eta}_t[n] \in \mathbb{C}^N,$$

where  $N$  is the number of transmit antennas and  $\boldsymbol{\eta}_t[n]$  is the transmitter noise, which will be referred to as *Tx-noise*. According to [2], Tx-noise is accurately modeled as an additive Gaussian-distributed noise, i.e.  $\boldsymbol{\eta}_t \sim \mathcal{N}_{\mathbb{C}}(\mathbf{0}, \mathbf{C}_{\eta_t})$ , where  $\mathbf{C}_{\eta_t}$  is the Tx-noise covariance matrix. It is also assumed that Tx-noise is independent from the transmitted signals. Correspondingly, we define the *Signal-to-Tx-Noise Ratio* (STxNR) as

$$\text{STxNR} = \frac{E_{tx}}{\text{tr}(\mathbf{C}_{\eta_t})},$$

where  $E_{tx}$  is the transmit energy and  $\text{tr}(\bullet)$  denotes the trace operator. In practical implementations, typical values of STxNR range between 22 dB and 32 dB [2].

## 3. MIMO THP DESIGN WITH TX-NOISE

Figure 1 shows the block diagram of a MIMO system with  $K$  receive antennas employing THP, which is a nonlinear precoding technique made up of a feedforward filter  $\mathbf{F} \in \mathbb{C}^{N \times K}$ , a backward filter  $\mathbf{I} - \mathbf{B} \in \mathbb{C}^{K \times K}$ , and a modulo operator, denoted in Fig. 1 by  $\mathbf{M}(\bullet)$ . The modulo operator is introduced to avoid the increase in transmit power due to the feedback loop [4]. Therefore, the modulo operator constrains the real and imaginary part of the signal at its input to the interval  $[-\tau/2, \tau/2]$  by adding integer multiples of  $\tau$  and  $j\tau$  to the real and imaginary part, respectively. Note that the parameter  $\tau$  depends on the modulation. In the particular case of QPSK modulation,  $\tau = 2\sqrt{2}$ . Data symbols sent from the transmitter to the  $K$  antenna receiver will be represented by  $\mathbf{u}[n] \in \mathbb{A}^K$ , where  $\mathbb{A}$  denotes the modulation alphabet. The ordering considerably affects the performance of THP and for this reason, transmit symbols are passed through a permutation filter  $\mathbf{P}$ . Minimization is carried out under the restriction of  $\mathbf{B}$  being a spatially causal filter and constrained transmit energy (i.e.  $E[\|\mathbf{x}[n]\|_2^2] = E_{tr}$ ) where  $\mathbf{x}[n] = \mathbf{F}\mathbf{v}[n] \in \mathbb{C}^N$  with  $\mathbf{v}[n]$  representing the output of the modulo operator in the transmit signal.

At reception, we assume that all acquired signals are scaled by the same positive real-valued factor  $g$ . This assumption is necessary in order to arrive at closed-form and unique solutions for the *Minimum Mean Square Error* (MMSE) THP design. According to our signal model, the received signal is

$$\hat{\mathbf{d}}_t[n] = \hat{\mathbf{d}}[n] + g\mathbf{H}\boldsymbol{\eta}_t[n] \in \mathbb{C}^K,$$

where  $\hat{\mathbf{d}}[n] = g\mathbf{H}\mathbf{F}\mathbf{v}[n] + g\boldsymbol{\eta}_r[n]$  is the received signal when there is no Tx-noise. At the receiver, the modulo operator

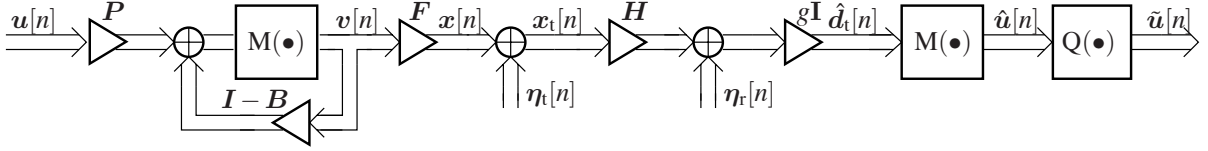


Figure 1: Block diagram of Tomlinson-Harashima precoding with Tx-noise.

is applied again to invert the effect of this operator at the transmitter and the resulting signal is passed through a symbol detector (represented by  $Q(\bullet)$  in Fig. 1) to produce the detected symbols  $\tilde{\mathbf{u}}[n] \in \mathbb{A}^K$ .

As explained in [5], the MMSE THP design searches for the filtering and permutation matrices that minimize the variance of the error vector

$$\epsilon_t[n] = \mathbf{P}^T \mathbf{B} \mathbf{v}[n] - \hat{\mathbf{d}}_t[n] = \epsilon[n] - g \mathbf{H} \boldsymbol{\eta}_t[n], \quad (1)$$

where  $\epsilon[n] = \mathbf{P}^T \mathbf{B} \mathbf{v}[n] - g \mathbf{y}[n]$  is the error vector when there is no Tx-noise.

Since transmitter noise is independent from transmitted signals and receiver noise, the MSE can be decomposed as

$$\text{MSE}_{t,\text{THP}} = \text{MSE}_{\text{THP}} + |g|^2 \text{tr}(\mathbf{H} \mathbf{C}_{\boldsymbol{\eta}_t} \mathbf{H}^H), \quad (2)$$

where  $\text{MSE}_{\text{THP}} = \mathbb{E}\{|\epsilon[n]|^2\}$  is the MSE when there is no Tx-noise, which constitutes the cost function that is minimized in the conventional MMSE design of THP [5], and  $\text{MSE}_{t,\text{THP}} = \mathbb{E}\{|\epsilon_t[n]|^2\}$  is the resulting MSE under transmitter noise conditions, with the error vector  $\epsilon_t[n]$  defined in Eq. (1).  $\mathbf{C}_{\boldsymbol{\eta}_r} = \mathbb{E}\{\boldsymbol{\eta}_r[n] \boldsymbol{\eta}_r^H[n]\}$  is the spatial covariance matrix of the *Additive White Gaussian Noise* (AWGN) at the receiver (so-called receiver noise, which is referred to as *Rx-noise*).

Following similar derivations to those in [5], the minimization of the MSE cost function of Eq. (2), subject to the mentioned constraints, can be carried out by means of the factorization of

$$\boldsymbol{\Phi}_t = (\mathbf{H} \mathbf{H}^H + \xi_t \mathbf{I})^{-1},$$

where

$$\xi_t = \xi + \text{tr}(\mathbf{H} \mathbf{C}_{\boldsymbol{\eta}_t} \mathbf{H}^H) / E_{\text{tx}}, \quad (3)$$

with  $\xi = \text{tr}(\mathbf{C}_{\boldsymbol{\eta}_t}) / E_{\text{tx}}$  [5]. The symmetrically permuted Cholesky decomposition of this matrix is

$$\mathbf{P} \boldsymbol{\Phi}_t \mathbf{P}^T = \mathbf{L}^H \mathbf{D} \mathbf{L}, \quad (4)$$

where  $\mathbf{L}$  and  $\mathbf{D}$  are, respectively, unit lower triangular and diagonal matrices. Finally, the MMSE solution for the THP filters that account for the Tx-noise is given by

$$\begin{aligned} \mathbf{F}_{\text{MMSE}}^{\text{THP}} &= g_{\text{MMSE}}^{\text{THP},-1} \mathbf{H}^H \mathbf{P}^T \mathbf{L}^H \mathbf{D} \\ \mathbf{B}_{\text{MMSE}}^{\text{THP}} &= \mathbf{L}^{-1}. \end{aligned}$$

The receive scalar weight  $g_{\text{MMSE}}^{\text{THP}}$  is directly obtained from the transmit energy constraint. Assuming that it is real-valued and positive, it is obtained that

$$g_{\text{MMSE}}^{\text{THP}} = \sqrt{\frac{\text{tr}(\mathbf{H}^H \mathbf{P}^T \mathbf{L}^H \mathbf{D}^2 \mathbf{C}_v \mathbf{L} \mathbf{P} \mathbf{H})}{E_{\text{tx}}}},$$

where  $\mathbf{C}_v$  is the covariance matrix of  $\mathbf{v}[n]$ , which is diagonal with entries depending on the modulation alphabet [4].

The minimum value for the MSE cost function given by Eq. (2) can be obtained by substituting the expressions obtained for the optimum filters  $\mathbf{F}_{\text{MMSE}}^{\text{THP}}$  and  $\mathbf{B}_{\text{MMSE}}^{\text{THP}}$ , and for the gain factor  $g_{\text{MMSE}}^{\text{THP}}$ . It is easy to show that the final MMSE under the presence of Tx-noise is given by

$$\text{MMSE}_{\text{THP}} = \xi_t \text{tr}(\mathbf{C}_v \mathbf{D}), \quad (5)$$

where  $\xi_t$  is given by Eq. (3) and  $\mathbf{D}$  is the diagonal matrix that results from the permuted Cholesky factorization of Eq. (4).

As done in [9], instead of testing all possible permutation matrices to find the one that minimizes the cost function of Eq. (5), the ordering optimization (given by the permutation matrix  $\mathbf{P}$ ) is included into the computation of the Cholesky decomposition of Eq. (4) (see [9]).

As in [5], it is straightforward to obtain the expressions for the ZF-THP design as the limiting case when  $\xi_t \rightarrow 0$ . The expressions for the filters  $\mathbf{F}_{\text{ZF}}^{\text{THP}}$  and  $\mathbf{B}_{\text{ZF}}^{\text{THP}}$  are equal to that obtained for  $\mathbf{F}_{\text{MMSE}}^{\text{THP}}$  and  $\mathbf{B}_{\text{MMSE}}^{\text{THP}}$ , respectively, although the matrices  $\mathbf{P}$ ,  $\mathbf{L}$ , and  $\mathbf{D}$  should be obtained from the symmetrically permuted Cholesky factorization of

$$\boldsymbol{\Phi}_t = (\mathbf{H} \mathbf{H}^H)^{-1}.$$

#### 4. MIMO VP DESIGN WITH TX-NOISE

Figure 2 shows the block diagram of a MIMO system including a vector precoder. The transmitter has the freedom to add an arbitrary perturbation signal  $\mathbf{a}[n] \in \tau \mathbb{Z}^K + j \tau \mathbb{Z}^K$  to the data signal prior to linear transformation with the filter  $\mathbf{F} \in \mathbb{C}^{N \times K}$ , since the receiver applies the modulo operator  $M(\bullet)$ . As in THP,  $\tau$  denotes a constant that depends on the modulation alphabet associated with the modulo operator.

As it can be seen from Fig. 2, the data vector  $\mathbf{u}[n] \in \mathbb{C}^K$  is first superimposed with the perturbation vector  $\mathbf{a}[n]$ , and the resulting vector is then processed by the linear filter  $\mathbf{F}$  to form the transmit vector  $\mathbf{x}[n] = \mathbf{F} \mathbf{d}[n] \in \mathbb{C}^N$ , where  $\mathbf{d}[n]$  is the desired signal given by  $\mathbf{u}[n] + \mathbf{a}[n]$  and  $n$  is the symbol index in a block size of  $N_B$  data symbols. The transmit energy constraint is expressed as  $\sum_{n=1}^{N_B} \|\mathbf{x}[n]\|_2^2 / N_B \leq E_{\text{tx}}$  since transmit symbols statistics are unknown.

The weight  $g$  in Fig. 2 is assumed to be constant throughout the block of  $N_B$  symbols. Again, note that we use a common weight for all the receive antennas. Thus, the weighted estimated signal is given by

$$\hat{\mathbf{d}}_t[n] = \hat{\mathbf{d}}[n] + g \mathbf{H} \boldsymbol{\eta}_t[n],$$

with  $\hat{\mathbf{d}}[n] = g \mathbf{H} \mathbf{F} \mathbf{d}[n] + g \boldsymbol{\eta}[n]$ . The modulo operator at the receiver is used to compensate the effect of adding the perturbation  $\mathbf{a}[n]$  at the transmitter.

The procedure to obtain the optimum VP parameters is the following. We start by fixing  $\mathbf{a}$ , after which  $\mathbf{x}$  and  $g$  are

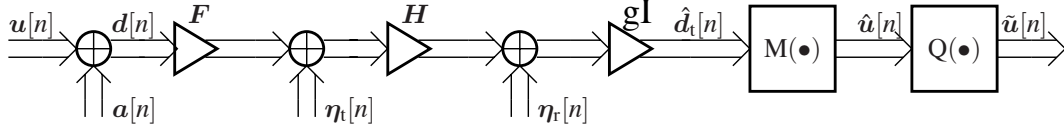


Figure 2: Block diagram of vector precoding with Tx-noise.

optimized taking into account the transmit power constraint. For these optimum  $\mathbf{x}$  and  $g$  we choose the best  $\mathbf{a}$  according to the *Mean Square Error* (MSE) criterion [6].

As it is demonstrated in [6], the MSE can be expressed as

$$\text{MSE}_{t,\text{VP}} = \text{MSE}_{\text{VP}} + \frac{1}{N_B} \sum_{n=1}^{N_B} \|g\mathbf{H}\boldsymbol{\eta}_t[n]\|_2^2, \quad (6)$$

where  $\text{MSE}_{\text{VP}} = \sum_{n=1}^{N_B} \mathbb{E}[\|\mathbf{d}[n] - \hat{\mathbf{d}}[n]\|_2^2] \mathbf{u}[n] / N_B$  with no Tx-noise, and  $\text{MSE}_{t,\text{VP}} = \sum_{n=1}^{N_B} \mathbb{E}[\|\mathbf{d}[n] - \hat{\mathbf{d}}[n]\|_2^2] \mathbf{u}[n] / N_B$ , otherwise. Then, we reach the following solution for the MMSE vector precoder

$$\begin{aligned} \mathbf{x}_{\text{MMSE}}^{\text{VP}}[n] &= g_{\text{MMSE}}^{-1,\text{VP}} (\mathbf{H}^H \mathbf{H} + \xi_t \mathbf{I})^{-1} \mathbf{H}^H \mathbf{d}[n] \\ g_{\text{MMSE}}^{\text{VP}} &= \sqrt{\frac{\sum_{n=1}^{N_B} \mathbf{d}^H[n] \mathbf{H} (\mathbf{H}^H \mathbf{H} + \xi_t \mathbf{I})^{-2} \mathbf{H}^H \mathbf{d}[n]}{E_{\text{tx}} N_B}}, \end{aligned} \quad (7)$$

where  $g_{\text{MMSE}}^{\text{VP}}$  is directly obtained from the transmit energy constraint.

By defining the matrix  $\boldsymbol{\Phi}_t = (\mathbf{H}^H \mathbf{H} + \xi_t \mathbf{I})^{-1}$  and applying the matrix inversion lemma to  $\mathbf{x}_{\text{MMSE}}^{\text{VP}}[n]$  in Eq. (7), the MSE expression of Eq. (6) is reduced to [6]

$$\text{MMSE}_{t,\text{VP}} = \frac{\xi_t}{N_B} \sum_{n=1}^{N_B} \mathbf{d}^H[n] \boldsymbol{\Phi}_t \mathbf{d}[n].$$

Since  $\boldsymbol{\Phi}_t$  is positive definite, we can use the Cholesky factorization to obtain a lower triangular matrix  $\mathbf{L}$  and a diagonal matrix  $\mathbf{D}$  with the following relationship [6],

$$\boldsymbol{\Phi}_t = (\mathbf{H}^H \mathbf{H} + \xi_t \mathbf{I})^{-1} = \mathbf{L}^H \mathbf{D} \mathbf{L}.$$

Thus, the perturbation signal can be found by the following search [6]

$$\begin{aligned} \mathbf{a}_{\text{MMSE}}^{\text{VP}}[n] &= \underset{\mathbf{a}[n] \in \tau\mathbb{Z}^K + j\tau\mathbb{Z}^K}{\text{argmin}} (\mathbf{u}[n] + \mathbf{a}[n])^H \boldsymbol{\Phi}_t (\mathbf{u}[n] + \mathbf{a}[n]) \\ &= \underset{\mathbf{a}[n] \in \tau\mathbb{Z}^K + j\tau\mathbb{Z}^K}{\text{argmin}} \|\mathbf{D}^{1/2} \mathbf{L} (\mathbf{u}[n] + \mathbf{a}[n])\|_2^2, \end{aligned}$$

which can be solved by means of the Schnorr-Euchner sphere decoding algorithm [10, 11]. The successive computation of  $\mathbf{a}[n]$  leads to the suboptimum approach of THP described above.

The ZF constraint  $\mathbb{E}[\hat{\mathbf{d}}[n] | \mathbf{d}[n]] = g\mathbf{H}\mathbf{F}\mathbf{d}[n]$ , for  $n = 1, \dots, N_B$ , leads to similar expressions for  $\mathbf{x}_{\text{ZF}}^{\text{VP}}[n]$  and  $g_{\text{ZF}}^{\text{VP}}$  as those obtained for the MMSE-VP design in Eq. (7) but considering  $\xi_t \rightarrow 0$ . Following similar steps as before, the MMSE for ZF-VP has exactly the same form as for MMSE-VP redefining  $\boldsymbol{\Phi}_t$  as  $(\mathbf{H}^H \mathbf{H})^{-1}$ . Finally, the optimum perturbation vectors are found by the following closest point search in a lattice [6]

$$\mathbf{a}_{\text{ZF}}^{\text{VP}}[n] = \underset{\mathbf{a}[n] \in \tau\mathbb{Z}^K + j\tau\mathbb{Z}^K}{\text{argmin}} \left\| \mathbf{H}^H (\mathbf{H}^H \mathbf{H})^{-1} \mathbf{d}[n] \right\|_2^2.$$

## 5. SIMULATION RESULTS

In this section, the results of several computer simulations are presented to illustrate the impact of Tx-noise on the performance of the MIMO precoding schemes described in the previous sections. We consider two types of channels: synthetically-generated spatially-white Rayleigh channels and channels measured using a testbed in an indoor scenario at the University of A Coruña [3] by considering  $N = 4$  and  $K = 4$  transmit and receive antennas, respectively. The performance metric is the uncoded *Bit Error Rate* (BER) versus the *Signal-to-Rx-Noise Ratio* (SRxNR) defined as

$$\text{SRxNR} = \frac{E_{\text{tx}} K}{\text{tr}(\mathbf{C}_{\eta_r})},$$

where  $\mathbf{C}_{\eta_r}$  is the Rx-noise covariance matrix. The Rx-noise is also assumed to be statistically independent from the Tx-noise. We assume the presence of residual Tx-impairments that produce a STxNR of 25 dB, which lies in the practical range between 22 dB and 32 dB. The symbols are QPSK modulated and it is also assumed that  $\mathbf{C}_u = \mathbf{I}$ . The channel is quasi-static and remains unchanged during the transmission of a symbol frame, although it changes in an statistically-independent fashion between frames.

### 5.1 Results for Spatially-White Rayleigh Channels

Figures 4 and 5 plot BER versus SRxNR for a  $4 \times 4$  MIMO system with THP and VP setups, respectively. The channel has been synthetically generated from a set of i.i.d. complex-valued Gaussian random variables (i.e. it is a spatially-white MIMO Rayleigh channel). In this subsection we assumed both receiver and transmitter noise are spatially-white, i.e.  $\mathbf{C}_{\eta_t} = \sigma_t^2 \mathbf{I}$  and  $\mathbf{C}_{\eta_r} = \sigma_r^2 \mathbf{I}$ . A hundred channel realizations are considered with frames of  $10^6$  symbols.

Note that the impact of the Tx-noise is extremely important on the performance of THP, as shown in Fig. 4. The performance of conventional THP severely degrades for SRxNR values above 25 dB, where Tx-noise causes an error floor of about  $10^{-3}$ . As it can be seen from the figure, the classical MMSE curve with Tx-noise goes up again at high SRxNR since MMSE-THP converges to ZF-THP, which is much more sensitive to noise. Notice that the effect of Tx-noise could be seen as an additive and coloured noise at the receiver. However, note that including Tx-noise into the MMSE-THP design greatly alleviates this problem and the error floor is reduced to a residual value of about  $10^{-7}$ . For vector precoding, as it can be seen from Fig 5, the BER performance is much less affected by Tx-noise than in the case of THP. Nevertheless, the inclusion of Tx-noise in filter optimizations improves the performance achieved by classical VP designs in 1 dB at a BER of  $10^{-6}$ .

### 5.2 Results for Measured Indoor Channels

We also carried out computer experiments considering channels measured in a realistic indoor scenario with a testbed

$$\hat{\mathbf{C}}_{\eta_r} = 10^2 \times \begin{bmatrix} 1.2058 & -0.0104 + 0.0079i & -0.0030 + 0.0141i & 0.0212 - 0.0040i \\ -0.0104 - 0.0079i & 0.9973 & 0.0119 + 0.0061i & 0.0043 - 0.0038i \\ -0.0030 - 0.0141i & 0.0119 - 0.0061i & 0.6265 & -0.0007 + 0.0076i \\ 0.0212 + 0.0040i & 0.0043 + 0.0038i & -0.0007 - 0.0076i & 1.1025 \end{bmatrix},$$

$$\hat{\mathbf{C}}_{\eta_t} = 10^{-3} \times \begin{bmatrix} 2.6069 & 0.0810 - 0.0115i & 0.0058 + 0.0068i & -0.0107 + 0.0001i \\ 0.0081 + 0.0115i & 2.6413 & 0.0020 + 0.0020i & -0.0127 + 0.0035i \\ 0.0058 - 0.0068i & 0.0020 - 0.0020i & 2.5552 & 0.0037 + 0.0018i \\ -0.0107 - 0.0001i & -0.0127 - 0.0035i & 0.0037 - 0.0018i & 3.4155 \end{bmatrix}.$$

Figure 3: Transmitter and receiver noise covariance matrices estimated using the testbed.

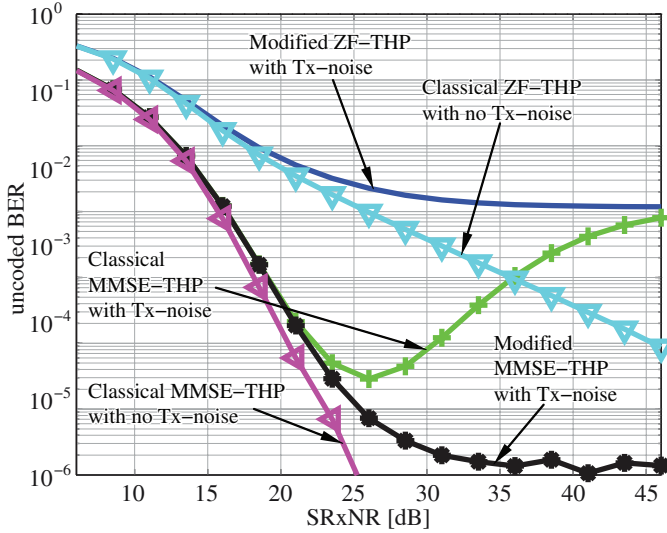


Figure 4: BER vs. SRxNR with Tomlinson-Harashita over spatially-white Rayleigh channels.

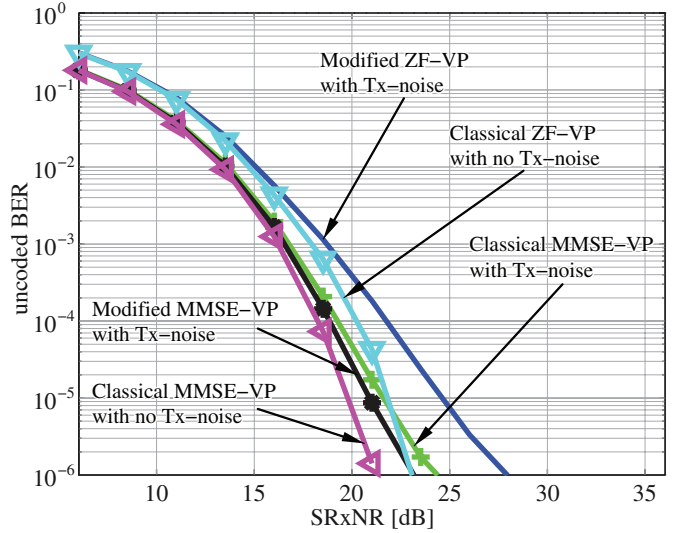


Figure 5: BER vs. SRxNR with vector precoding over spatially-white Rayleigh channels.

developed at the University of A Coruña [3]. The testbed is made up of two PCs, one for the transmitter and one for the receiver. Each PC contains the baseband hardware plus the *Radio-Frequency Front-End* (RF-FE). The baseband hardware is composed of fast memories, which can be accessed at the speed of the A/D and D/A converters, thus allowing the transmission and subsequent acquisition of signals in real-time. However, the signal processing at both transmitter and receiver sides is performed off-line.

With the goal of obtaining statistically rich channel realizations, and given that the utilized RF-FE is frequency-agile, we measure at different RF carriers in the frequency interval ranging from 5219 MHz to 5251 MHz and from 5483 MHz to 5703 MHz. Carrier spacing is 4 MHz (greater than the signal bandwidth, which is equal to 1.12 MHz), resulting in 65 different frequencies. Additionally, we repeat the whole measurement procedure for four different positions of the receiver, giving as a result 260 channel realization measurements. After normalization, channel matrices have a mean Frobenius norm equal to  $NK = 16$ .

Figure 6 shows the frame structure, where a *Pseudo-Noise* (PN) sequence of 119 symbols is added as a preamble for synchronization together with a silence of 50 symbols. The receiver noise covariance matrix  $\hat{\mathbf{C}}_{\eta_r}$  is calculated based on the observations acquired during the silence after the preamble. On the other hand, both the MIMO channels and the total noise covariance matrix  $\hat{\mathbf{C}}_{\eta_{\text{tot}}}$  were esti-



Figure 6: Frame structure used by the measurement procedure.

mated during the transmission of the training sequence. The transmitter noise covariance matrix is directly obtained from  $\hat{\mathbf{C}}_{\eta_{\text{tot}}} = \hat{\mathbf{H}}\hat{\mathbf{C}}_{\eta_t}\hat{\mathbf{H}}^H + \hat{\mathbf{C}}_{\eta_r}$  by performing  $\hat{\mathbf{C}}_{\eta_t} = \hat{\mathbf{H}}^{-1}(\hat{\mathbf{C}}_{\eta_{\text{tot}}} - \hat{\mathbf{C}}_{\eta_r})\hat{\mathbf{H}}^{-H}$ . Figure 3 shows the receiver and transmitter noise covariance matrices obtained from the testbed measurements. These covariance matrices are plugged into the THP and VP filter expressions derived in the previous sections. Simulated Gaussian noise was additionally injected to change the operating SRxNR value.

Figure 7 plots the BER performance in terms of SRxNR for MIMO systems with both MMSE- and ZF-THP when transmitting over indoor channels obtained from the testbed. Two hundred and sixty channel realizations are considered with frames of  $10^5$  symbols. Again, note the high sensitivity of the performance of MIMO systems with THP with respect to Tx-noise. The performance of both MMSE- and ZF-THP is considerably degraded due to Tx-noise and an error floor arises at the significant BER value of  $2 \times 10^{-3}$ . This error floor can be reduced to the BER value of  $3 \times 10^{-6}$  when Tx-noise is considered in the design. The same effect is observed for VP over indoor channels but at lower values of BER since

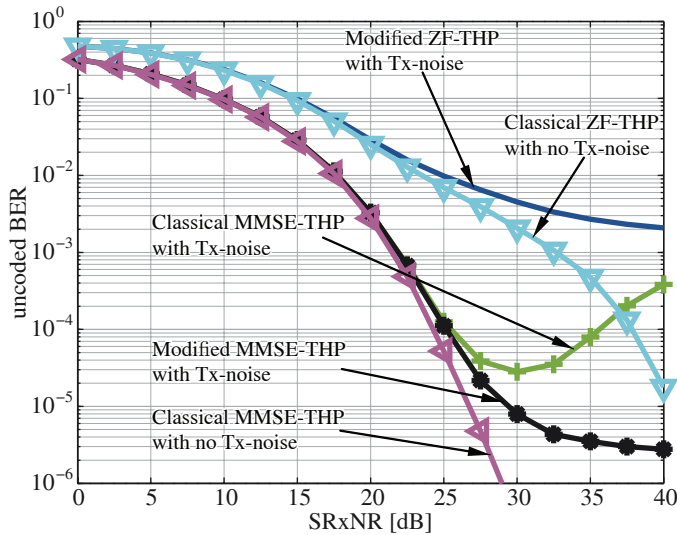


Figure 7: BER vs. SRxNR with Tomlinson-Harashima precoding over measured indoor channels.

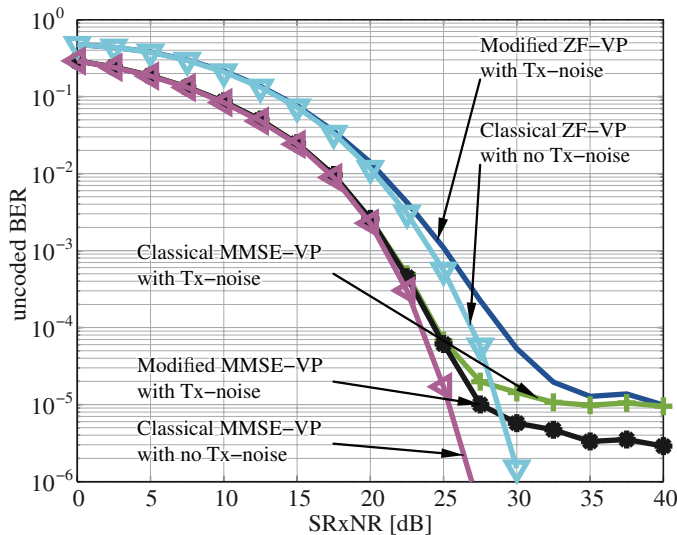


Figure 8: BER vs. SRxNR with vector precoding over measured indoor channels.

VP is optimal with respect to THP and not so influenced by noise impairments at the transmitter because of the correction performed by the lattice search. Figure 9 shows the histogram of the modulus and the angle of the measured MIMO channel coefficients. While the angle follows a uniform distribution, the modulus is clearly not Rayleigh. This explains the differences in performance between the case of measured indoor channels and that of spatially-white channels in the previous subsection.

## 6. CONCLUSIONS

This work investigates the impact of noise generated by practical transmitters on the performance of MIMO systems with nonlinear THP and VP. We have shown that Tx-noise severely degrades the performance of both precoding methods although their performance can be significantly improved if Tx-noise is included in precoder designs.

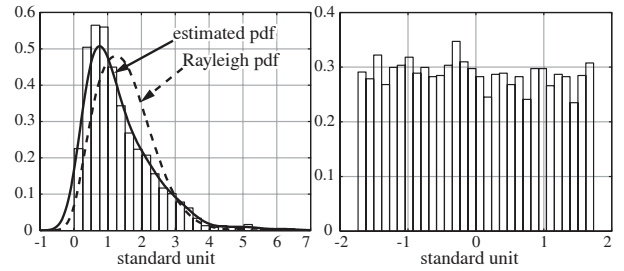


Figure 9: Histogram of the module (left-hand) and the angle (right-hand) of the estimated channel coefficients.

## Acknowledgments

This work has been funded by Xunta de Galicia, Ministerio de Ciencia e Innovación of Spain, and FEDER funds of the European Union under grants with numbers 10TIC003CT, 09TIC008105PR, TEC2010-19545-C04-01, and CSD2008-00010.

## REFERENCES

- [1] H. Suzuki, T.V.A. Tran, I.B. Collings, G. Daniels, and M. Hedley, "Transmitter Noise Effect on the Performance of a MIMO-OFDM Hardware Implementation Achieving Improved Coverage," *IEEE Journal on Selected Areas in Communications*, vol. 26, no. 6, pp. 867–876, Aug. 2008.
- [2] C. Studer, M. Wenk, and A. Burg, "MIMO Transmission with Residual Tx-RF Impairments," *International ITG Workshop on Smart Antennas*, pp. 189–196, February 2010.
- [3] J. A. García-Naya, M. González-López, and L. Castedo, *Radio Communications*, chapter A Distributed Multilayer Software Architecture for MIMO Testbeds, In-Tech, Apr. 2010.
- [4] R. F. H. Fischer, *Precoding and Signal Shaping for Digital Transmission*, John Wiley & Sons, 2002.
- [5] M. Joham, *Optimization of Linear and Nonlinear Transmit Signal Processing. PhD dissertation*, Munich University of Technology, 2004.
- [6] D. A. Schmidt, M. Joham, and W. Utschick, "Minimum Mean Square Error Vector Precoding," *European Transactions on Telecommunications*, vol. 19, no. 3, pp. 219–231, March/April 2008.
- [7] J. González-Coma, P. Castro, and L. Castedo, "Impact of transmit impairments on multiuser mimo non-linear transceivers," in *Proc. International ITG Workshop on Smart Antennas*, February 2011.
- [8] J. González-Coma, P. Castro, and L. Castedo, "Transmit impairments influence on the performance of mimo receivers and precoders," in *Proc. European Wireless*, April 2011.
- [9] K. Kusume, M. Joham, W. Utschick, and G. Bauch, "Cholesky factorization with symmetric permutation applied to detecting and precoding spatially multiplexed data streams," *IEEE Transactions on Signal Processing*, vol. 55, no. 6, pp. 3089–3103, June 2007.
- [10] C. P. Schnorr and M. Euchner, "Lattice basis reduction: Improved practical algorithms and solving subset sum problems," *Math. Programming*, vol. 66, pp. 188–191, September 1994.
- [11] M. O. Damen, H. El Gamal, and G. Caire, "On maximum-likelihood detection and the search for the closest lattice point," *IEEE Transactions on Information Theory*, vol. 49, no. 10, pp. 2389–2402, 2003.